

Cell Cycle Perturbations Induced by Infection with the Coronavirus Infectious Bronchitis Virus and Their Effect on Virus Replication

Brian Dove,¹ Gavin Brooks,² Katrina Bicknell,² Torsten Wurm,^{3†} and Julian A. Hiscox^{1,4*}

Institute of Molecular and Cellular Biology, University of Leeds, Leeds, LS2 9JT, United Kingdom¹; School of Pharmacy, University of Reading, Reading RG6 6AJ, United Kingdom²; School of Animal and Microbial Sciences, University of Reading, Reading RG6 6AJ, United Kingdom³; and Astbury Centre for Structural Molecular Biology, University of Leeds, Leeds LS2 9JT, United Kingdom⁴

Received 6 October 2005/Accepted 2 February 2006

In eukaryotic cells, cell growth and division occur in a stepwise, orderly fashion described by a process known as the cell cycle. The relationship between positive-strand RNA viruses and the cell cycle and the concomitant effects on virus replication are not clearly understood. We have shown that infection of asynchronously replicating and synchronized replicating cells with the avian coronavirus infectious bronchitis virus (IBV), a positive-strand RNA virus, resulted in the accumulation of infected cells in the G₂/M phase of the cell cycle. Analysis of various cell cycle-regulatory proteins and cellular morphology indicated that there was a down-regulation of cyclins D1 and D2 (G₁ regulatory cyclins) and that a proportion of virus-infected cells underwent aberrant cytokinesis, in which the cells underwent nuclear, but not cytoplasmic, division. We assessed the impact of the perturbations on the cell cycle for virus-infected cells and found that IBV-infected G₂/M-phase-synchronized cells exhibited increased viral protein production when released from the block when compared to cells synchronized in the G₀ phase or asynchronously replicating cells. Our data suggested that IBV induces a G₂/M phase arrest in infected cells to promote favorable conditions for viral replication.

Many viruses interact with the cell cycle, and examples can be found from DNA viruses, retroviruses, and RNA viruses. The cell cycle can be divided into a number of separate events (43): DNA replication (S phase), nuclear division (mitosis [M]), and cell division (cytokinesis), separated by two gap periods (G₁ and G₂). Quiescent cells are described as being in G₀. Progression through each phase of the cycle and from one phase to the next is tightly regulated and highly orchestrated, being controlled by cyclins and cyclin-dependent kinases as well as other factors. Cyclin D/CDK4 (CDK6) complexes initiate progression through G₁ by phosphorylating substrates, which eventually leads to the transcription activation of genes necessary for DNA synthesis and subsequent cell cycle progression; the cyclin E/CDK2 complex is important in the G₁/S transition, where levels peak at the restriction point; cyclin A/CDK2 is important during S-phase progression; and cyclin B/CDK2 complexes are important for progression through late G₂ and early M. Cytokinesis can be viewed as the final stage of the cell cycle and is the programmed division of a cell into two daughter cells, each containing one nucleus (13). There are many cell cycle-regulatory molecules, including the tumor suppressor protein p53, which acts as a suppressor through its capacity to induce apoptosis and cell cycle arrest (26). The activity of p53 can be governed by its subcellular localization and the stress state of the cell (37, 52).

Alteration of the host cell cycle by RNA viruses has not been described as extensively in the literature when compared to DNA viruses or retroviruses. For example, human immunodeficiency virus type 1 (HIV-1) Vpr arrests cells in the G₂ phase (16, 20, 44, 51), resulting in an increase in transcription (22) and virus production (11). In the case of positive-strand RNA viruses the possible relationship between virus-induced cell cycle perturbations and the concomitant effects on virus replication are not well understood. Coronaviruses are a group of positive-strand RNA viruses which replicate in the cytoplasm of infected cells. Coronaviruses, together with the closely related arteriviruses, belong to the *Nidovirales*. Several coronaviruses and/or their proteins have been shown to alter cell signaling, in some cases with implications for cell growth (6, 17, 60). In this study we tested the hypothesis that infection with the avian coronavirus infectious bronchitis virus (IBV) could perturb the cell cycle and that this would promote favorable conditions for progeny virus synthesis, which has not previously been established.

MATERIALS AND METHODS

Cells and viruses. Vero (an African green monkey kidney-derived epithelial cell line) and BHK-21 cells (a baby hamster kidney-derived fibroblast cell line) were maintained in Dulbecco's modified Eagle medium (DMEM) supplemented with 10% fetal calf serum (FCS). IBV Beaudette US, an IBV strain adapted for growth in Vero cells (1), was propagated in Vero cells, and the virus was harvested at 24 h postinfection (p.i.). Virus titer was calculated by plaque assay titration in Vero cells. All cell culture experiments in this study were conducted in the absence of antibiotic or antifungal agents and were performed on actively replicating subconfluent cells (i.e., not undergoing contact inhibition).

IBV infection of Vero cells. Flasks (75 cm²) were seeded with 1 × 10⁶ Vero or BHK-21 cells. At 60% confluence, cells were mock infected, exposed to UV-inactivated virus or infected with IBV with a multiplicity of infection (MOI) of 1, and then incubated for 1 h at 37°C, after which the cells were incubated in

* Corresponding author. Mailing address: Institute of Molecular and Cellular Biology, Faculty of Biological Sciences, University of Leeds, Leeds LS2 9JT, United Kingdom. Phone: 44 (0)113 343 5582. Fax: 44 (0)113 343 3167. E-mail: j.a.hiscox@leeds.ac.uk.

† Present address: Institute for Molecular Virology and McArdle Cancer Research Facility, University of Wisconsin-Madison, Madison, Wis.

maintenance media. Cells were processed at various times p.i. for Western blot and cell cycle flow-cytometric analysis and, at 24 h p.i., for confocal analysis.

UV inactivation of IBV. IBV was exposed to 120,000 mJ/cm² of 254-nm shortwave UV radiation for 10 min within a CL-1000 cross-linker (UVP). To demonstrate that IBV had been inactivated, Western blotting and reverse transcription-PCR (RT-PCR) were used to determine the presence or absence of viral proteins in cells infected with UV-inactivated virus. Total protein for Western blot analysis was prepared as described below, and total cellular RNA for RT-PCR was extracted using the RNeasy method (QIAGEN). RT-PCR amplification of a 415-bp IBV nucleocapsid (N) gene and 624-bp GAPDH (glyceraldehyde-3-phosphate dehydrogenase)-derived fragments was performed with *Taq* polymerase (Invitrogen).

G₀/G₁, G₁/S, and G₂/M Vero cell synchronization. Flasks (75 cm²) were seeded with 1 × 10⁶ Vero cells. Vero cells were G₀/G₁ phase synchronized using serum deprivation in cells in DMEM containing no FCS supplementation for 72 h. Vero cells were synchronized at the G₁/S phase border using double-thymidine treatment (15) by incubation for 12 h in maintenance media supplemented with 2 mM thymidine (Sigma). Cells were then washed three times with phosphate-buffered saline (PBS) and incubated for 12 h in maintenance media, followed by an additional 12-h incubation in maintenance media supplemented with 2 mM thymidine. Vero cells were G₂/M phase synchronized using nocodazole treatment by incubation of cells in maintenance media supplemented with 60 ng/ml nocodazole (Sigma) for 16 h. Immediately prior to mock infection and IBV infection of synchronized cells, serum-deprived cells were treated with DMEM supplemented with 10% FCS. Both thymidine- and nocodazole-treated cells were washed three times with PBS, and then the cell number per flask was determined and used to ensure an MOI of 0.1 or 1 between separate treatments. At various times p.i., cells were processed for Western blot and flow-cytometric analysis.

BrdU incorporation and flow cytometry analysis. Two-color flow-cytometric analysis was used to accurately determine the cell cycle profile of both mock-infected and infected cell populations. The principle of the technique is to use propidium iodide (PI) to stain DNA and thus measure those cells in G₀/G₁ (2N) and G₂/M (4N). Prior to staining, the thymidine analogue bromodeoxyuridine (BrdU) is incorporated into actively replicating DNA and thus accurately determines the proportion of cells in S phase. Two-color flow-cytometric analysis is advantageous when studying induced cell cycle perturbations, which can skew cell cycle data if profiles are determined using PI only (8, 9, 38, 40, 41). BrdU was added to cell medium within each flask to give a concentration of 10 μM BrdU, and medium was incubated at 37°C for 30 min to allow BrdU incorporation. Cells were washed once with PBS and then detached by the addition of 2 ml EDTA/trypsin and incubated for 5 min at 37°C. Vero cell growth medium was added to neutralize the trypsin, and cells were pelleted by centrifugation at 950 × *g* for 5 min and then fixed in 1 ml of 70% ethanol. BrdU-labeled cell samples in 70% ethanol solution were pelleted by centrifugation at 800 × *g* for 5 min and then incubated in 1 ml of 0.1 M HCl in PBS at 37°C for 10 min before addition of 3 ml of PBS. Samples were then pelleted by centrifugation at 800 × *g* for 5 min before addition of 100 μl of anti-BrdU solution (anti-BrdU antibody [BD Biosciences] diluted 1:5 in PBS, 0.5% Tween 20, and 1% fetal bovine serum [FBS]) and incubated for 60 min at 20°C. Samples were then washed in PBS, pelleted by centrifugation at 800 × *g* for 5 min before addition of 100 μl of anti-mouse fluorescein isothiocyanate (FITC)-labeled solution (antibody diluted 1:10 in PBS, 0.5% Tween 20, and 1% FBS) and incubated for 30 minutes in the dark at 20°C. Samples were washed twice in PBS before addition of 1 ml of PI staining solution (PBS, 50 μg/ml PI, 200 μg/ml RNase). Labeled cells were analyzed for PI staining and BrdU incorporation using a FACSCalibur analyzer (Becton Dickinson), and percentages of cells in the G₀/G₁, S, and G₂/M phases in each sample were determined by gating using CellQuest software (Becton Dickinson).

Preparation of protein lysates, Western blot analysis, and antibodies. Cells were lysed in radioimmunoprecipitation assay buffer (50 mM Tris-HCl, pH 7.5, 150 mM NaCl, 1% Nonidet P-40, 0.5% sodium deoxycholate, 0.1% sodium dodecyl sulfate [SDS]), supplemented with complete protease cocktail inhibitor (Roche), and the amount of protein in each sample was determined by bicinchoninic acid assay (Pierce). Ten or 20 μg of total cellular protein from each sample was separated on a 10% Novex Bis-Tris polyacrylamide precast gel in MES (morpholineethanesulfonic acid)-SDS running buffer (Invitrogen). Western blotting was performed using ECL (Amersham/Pharmacia) as described in the manufacturer's instructions. Rabbit anti-IBV polyclonal antisera (diluted 1:10,000) were used for the detection of IBV N protein (kindly donated by Dave Cavanagh, Institute for Animal Health, Compton, United Kingdom). Antibodies for the detection of p21 (C-19), p53 (D0-1), proliferating cell nuclear antigen (PCNA) (PC-10), cyclin A (H-432), cyclin E (M-20), cyclin D1 (M-20), cyclin D2 (M-20), cyclin D3 (M-10), and cyclin B1 (M-10) (all diluted 1:500) were obtained

from Santa Cruz Biotechnology. Anti-GAPDH (6C5) antibody (diluted 1:40,000) was obtained from AbCam. Horseradish peroxidase-conjugated goat anti-rabbit and rabbit anti-mouse secondary antibodies (diluted 1:1,000) (Sigma) were used as appropriate.

Confocal microscopy. Mock-infected and IBV-infected (MOI of 1) Vero cells were fixed at 24 h p.i., and confocal sections were captured on an LSM510 META microscope (Carl Zeiss Ltd.). IBV-infected cells were labeled with rabbit anti-IBV polyclonal sera (1:300) and detected with mouse anti-rabbit FITC (1:300) (green). The cell nucleus and nucleoli were stained with fluorescence grade PI (Molecular Probes), and where appropriate p53 was labeled with mouse anti-p53 monoclonal antibody (D01; Santa Cruz) and detected with Alexa Fluor goat anti-mouse 633 antibody (1:300; Molecular Probes) (red).

Statistical analysis. Statistical analysis was performed using the Student *t* test; a *P* value <0.05 was considered significant.

RESULTS

Infection of asynchronously dividing Vero and BHK cells with IBV results in an accumulation of cells in the G₂/M population and requires replicating virus. To investigate whether infection with IBV resulted in any changes to the cell cycle profile and whether these required replicating virus, flow-cytometric analysis was performed at 24 h p.i. on mock-infected cells, infected cells, and cells infected with UV-inactivated IBV. Two different cell types were utilized, Vero and BHK, which are permissive for IBV infection and have been used as model cell types to study virus-cell interactions (2, 6, 29, 42, 61). Three independent experiments, each containing triplicate samples, were conducted. The data indicated that there was no significant difference in cell cycle profiles between mock-infected cells and cells infected with UV-inactivated virus, although there was a significant increase in the G₂/M phase population between both Vero (*P* < 0.001) and BHK (*P* < 0.005) infected cells and cells receiving mock infection and UV-inactivated virus. Representative cell cycle profiles and histograms are shown for Vero (Fig. 1A) and BHK (Fig. 1B). UV inactivation of IBV was confirmed for Vero cells by the absence of either the N gene or N protein in UV-inactivated-IBV-treated cells compared to infected cells at 24 h postinfection (Fig. 1C and D). The cell cycle profiles of mock-infected cells and cells infected with UV-inactivated virus showed comparable levels of BrdU-labeled DNA in the S phase of the cell cycle. However, the cell cycle profiles of IBV-infected Vero cells demonstrated reduced BrdU labeling of DNA compared to mock-infected and UV-inactivated-virus-infected cells. The G₂/M phase arrest and concurrent reduced S phase DNA BrdU labeling observed in IBV-infected Vero cells occur as a result of replicating virus rather than viral attachment and/or entry and are not cell type dependent. Given that higher titers of IBV are obtained from Vero versus BHK cells (2), Vero cells were utilized in subsequent experiments.

To examine the initiation of virally induced cell cycle perturbations in actively replicating proliferating cells, Vero cells were infected with IBV or mock infected and cell cycle profiles determined by flow cytometry at 0, 4, 8, 12, 16, 20, and 24 h postinfection. Representative cell cycle profiles and histograms are presented in Fig. 2 and 3, respectively. Comparison of the cell cycle profiles between mock-infected and infected cells revealed that over the course of the infection there was a significant increase (*P* < 0.05, *n* = 3) in the proportion of cells in the G₂/M phases of the cell cycle in infected cells compared to mock-infected cells from 8 h postinfection. This G₂/M phase

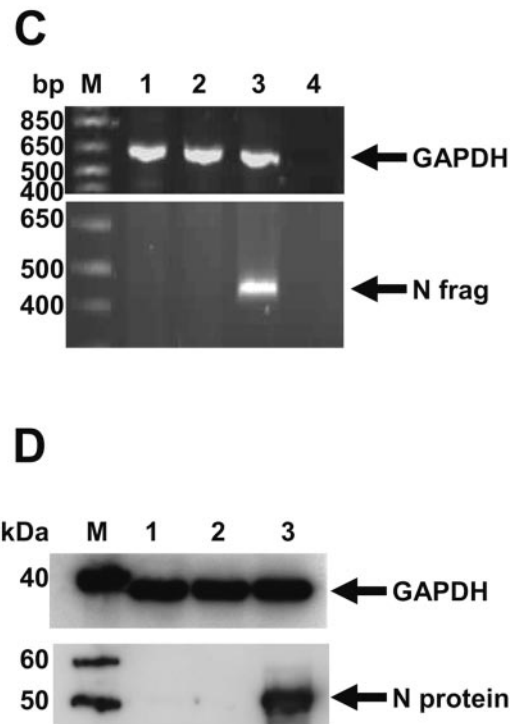
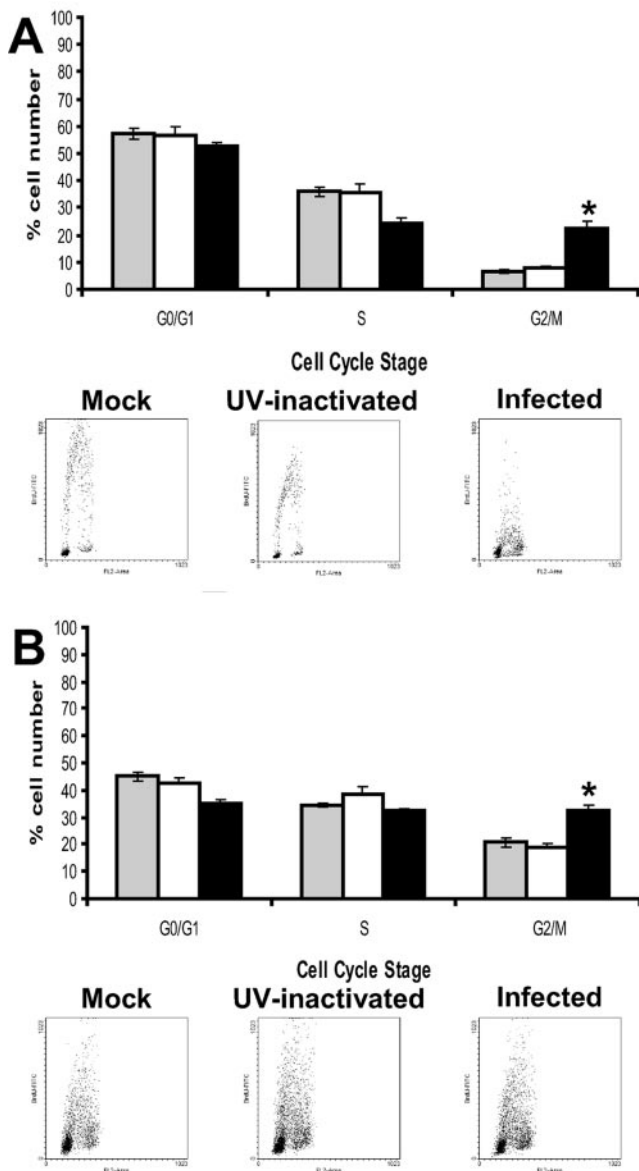


FIG. 1. IBV-induced G₂/M phase arrest is dependent upon the presence of replication-competent virus. Histogram of the mean percentage of mock-infected (gray), UV-inactivated-virus-infected (white), and IBV-infected (black) cells in the G₀/G₁, S, and G₂/M phases of the cell cycle after 24 h postinfection (± standard deviations). Significant differences between the numbers of IBV-infected G₂/M cells and the corresponding numbers of mock-infected and UV-inactivated-virus-infected cell controls for Vero ($P < 0.001, n = 3$) and BHK ($P < 0.05, n = 3$) are indicated by an asterisk. Similar results were obtained from three independent experiments. Representative dual-stained BrdU/PI cell cycle profiles are shown for mock-infected, UV-inactivated-virus-infected, and IBV-infected Vero (A) and BHK (B) cells at 24 p.i. (the x axis is the intensity of PI staining, and the y axis is the intensity of BrdU staining). (C and D) To ensure UV-inactivated IBV was incapable of replication or protein synthesis, cellular RNA and protein were isolated from mock-infected (lane 1), UV-inactivated-virus-infected (lane 2), and IBV-infected Vero cells (lane 3) and examined by (C) RT-PCR and (D) Western blotting for the presence of IBV N protein. The detection of GAPDH mRNA (C) and protein (D) was used as a control. Lane 4 in panel C is a negative control for RT-PCR.

increase in infected cells was not accompanied by a specific G₀/G₁ phase or S phase-only decrease over the length of the time course, although there were significant differences in populations at certain time points. Comparison of the cell cycle profiles also demonstrated a reduction in the level of BrdU incorporation in DNA in the S phase of the cell cycle in infected cells from 12 h postinfection.

IBV infection causes perturbations in the cell cycle machinery. We determined the level and activity of various cell cycle-regulatory factors at 0, 4, 8, 16, and 24 h p.i. in IBV-infected cells compared to mock-infected cells. Western blotting was performed to detect appropriate proteins. The level of GAPDH between the samples was used to demonstrate equal loading of proteins and for standardization of protein amounts for densitometry using Bio-Rad Quantity One software where appropriate. This experiment was conducted in triplicate, and representative Western blot data are presented in Fig. 4. To obtain a

measure of IBV infection, we used immunoblotting to detect the presence of N protein, which was observed at 4 h postinfection and increased throughout infection. To control protein loading and densitometric analysis, we analyzed the levels of GAPDH between mock-infected and infected samples. Western blot data indicated that there was no change in the level of GAPDH between mock-infected and infected cells at any of the time points analyzed. Between 0 and 8 h postinfection there appeared to be no difference in cyclin levels between mock-infected and infected cells. However, at 16 h postinfection levels of cyclins D1 and D2 appeared to be lower in infected cells compared to mock-infected cells, and this was also reflected in data taken at 24 h postinfection. Densitometric analysis indicated that cyclin D1 and D2 levels were 10- and 15-fold lower, respectively, in infected cells. Densitometric analysis showed that there was twofold-less cyclin E in infected cells at 24 h postinfection compared to mock-infected cells. With cyclins A and B1 at 24 h postinfection there was

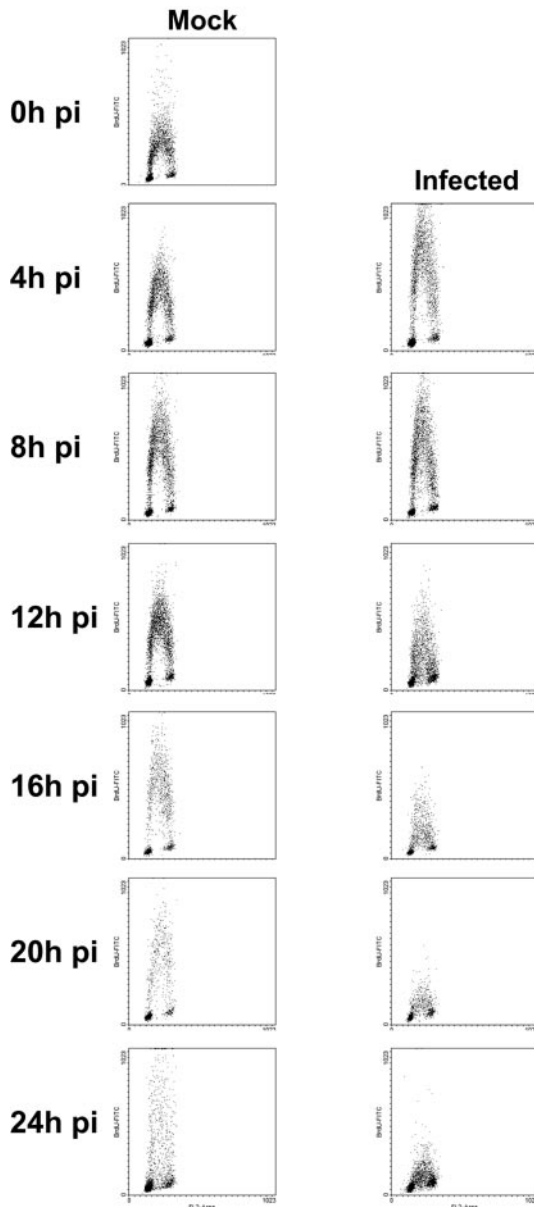


FIG. 2. Representative dual-stained BrdU/PI cell cycle profiles for mock- and IBV-infected Vero cells at 0, 4, 8, 12, 16, 20, and 24 h postinfection. Representative cell cycle profiles for mock- and IBV-infected Vero cells are shown to the left (the x axis is the intensity of PI staining, and the y axis is the intensity of BrdU staining).

2-fold-less cyclin A and 2.5-fold-less cyclin B1 in infected cells compared to mock-infected cells.

Our data indicate that infection with IBV leads to an accumulation of cells in the G_2/M phases of the cell cycle, with decreases in certain cell cycle factors and a reduction in BrdU uptake in cells undergoing S phase. Therefore, we examined the levels of p53 and p21, which are involved in the progression of G_1 into S phase and the G_2/M phase transition (57), and of PCNA, which is involved in DNA replication (48). Western blot and densitometric analysis indicated no difference in the levels of p53 in infected cells compared to mock-infected cells, and 2- and 2.5-fold reductions of p21 in infected cells com-

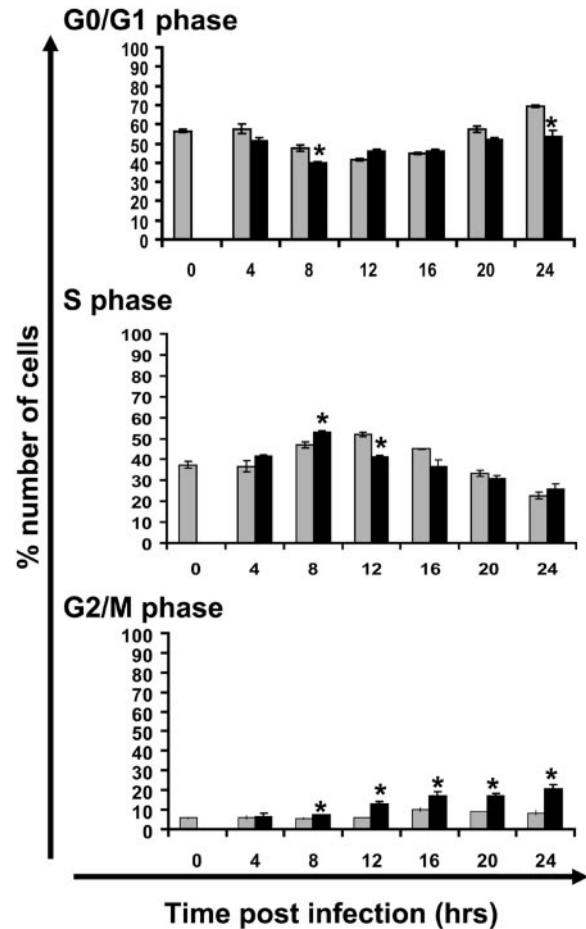


FIG. 3. IBV induces a G_2/M phase arrest in Vero cells. Cell cycle profiles for dual-stained BrdU/PI cells were analyzed by CellQuest software. Histogram bars represent the mean percentages of cells in the G_0/G_1 , S, and G_2/M phases of the cell cycle at 0, 4, 8, 12, 16, 20, and 24 h postinfection in mock-infected (gray) and IBV-infected (black) cells (\pm standard deviations). Significant differences ($P < 0.01$, $n = 3$) between data sets are indicated by an asterisk.

pared to mock-infected cells at 8 and 16 h postinfection, respectively, but not at 24 h postinfection. There was no difference in the amount of PCNA between mock-infected and infected cells at any time point analyzed.

Analysis of the morphology of virus-infected cells. Previously we have shown that IBV N protein causes aberrant cytokinesis in transfected cells. We examined the morphology of infected cells at 24 h postinfection using confocal microscopy to visualize viral proteins and the cell nucleus and nucleoli (16). Our analysis of several different fields of view and replicate infection with IBV indicated that approximately 15% of infected cells had undergone aberrant cytokinesis; two examples of these cells are presented in Fig. 5A to D and F to I. This was evidenced by the presence of a cleavage furrow, binucleate cells, and the nucleolus in each nucleus, which is visible using PI staining and also phase-contrast microscopy (Fig. 5J and K). To demonstrate that the cleavage furrow was present throughout the cell, we used the confocal microscope to construct a z section through the cell as shown in Fig. 5C; the cross section clearly shows the presence of the furrow though the axis of the cell (Fig.

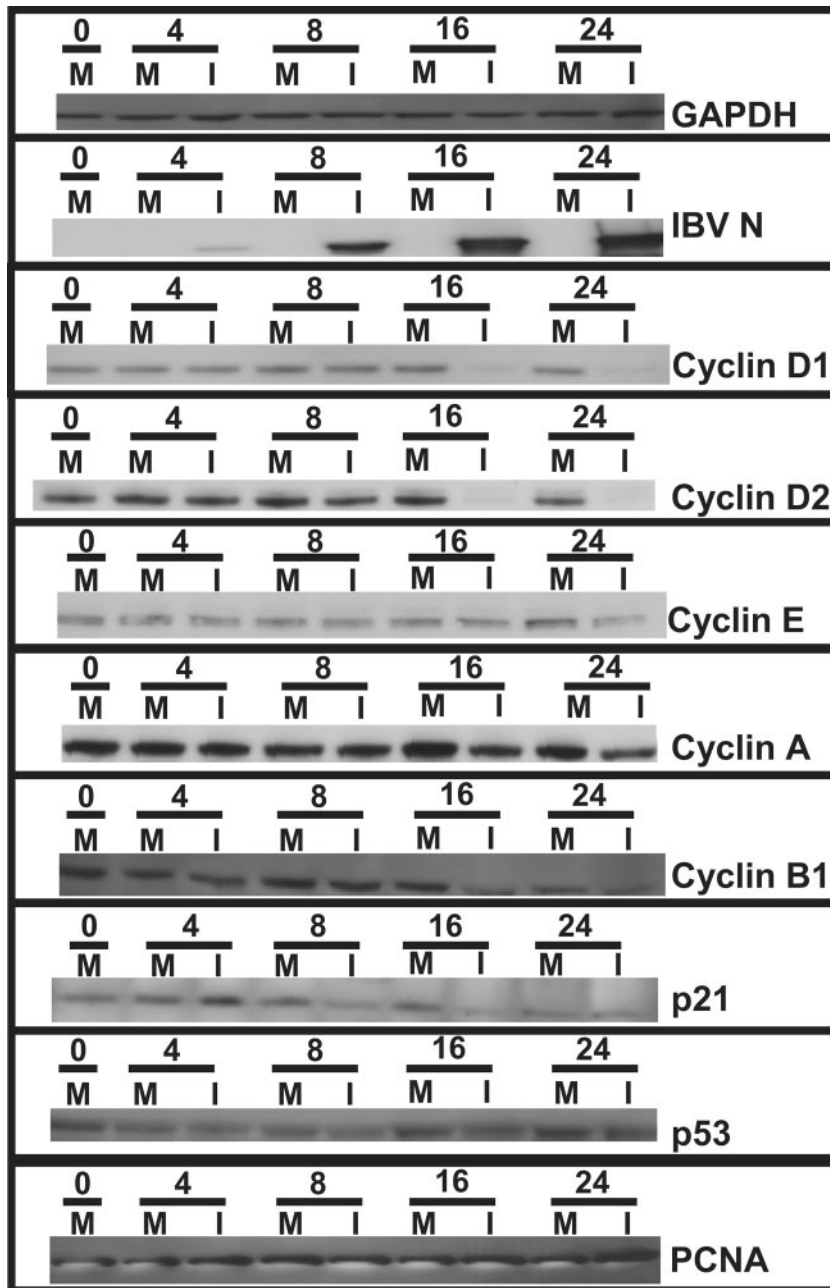


FIG. 4. Western blot analysis of total cellular protein isolated from mock (M)- and IBV-infected (I) Vero cells at 0, 4, 8, 16, and 24 h postinfection. Protein amounts were standardized as shown with GAPDH. Viral protein accumulation was confirmed by the detection of N protein, and several different proteins involved in various aspects of cell cycle control were analyzed, including G₁ cyclins (cyclins D1 and D2), a protein involved in G₁-to-S-phase progression (cyclin E), S phase (cyclin A and PCNA) and G₂/M (cyclin B1) proteins, and regulatory factors p21 and p53. This experiment was repeated three times, and representative blots are shown.

5E). Nucleoli are absent in normally dividing cells. To confirm these results, we used a marker protein for the nucleus, p53, rather than a postfixation stain. Detection of p53 (red) and IBV proteins (green) (Fig. 5L and M) also shows the presence of the cleavage furrow. Interestingly these merged images indicate that p53 was predominately located in the cytoplasm and had a punctate appearance in infected cells and that p53 and IBV proteins colocalize (as seen by the yellow signal). However, the IBV protein(s) which colocalizes with p53 could not

be identified, as the anti-IBV antibody used was a polyclonal antibody raised against the virus particle. In mock-infected cells p53 localized to the nucleolus, nucleus, and cytoplasm (data not shown).

G₂/M-phase-synchronized cells promote increased protein accumulation and progeny virus. Our data indicated that IBV caused an increase in the population of G₂/M phase cells in virus-infected cells and that this was not at the expense of either specifically the G₀/G₁ or S phase population (Fig. 1 and

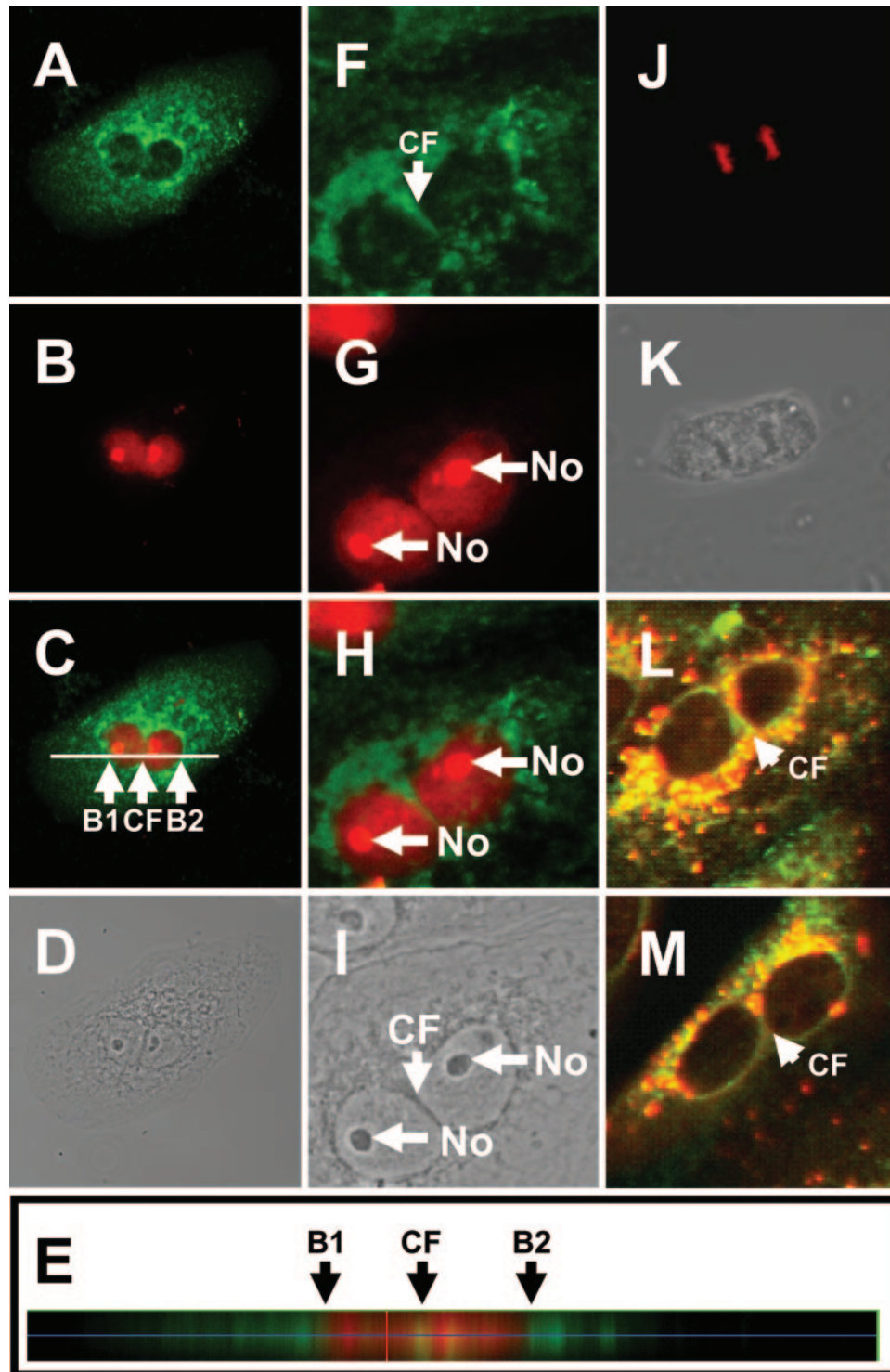


FIG. 5. Vero cells were infected with IBV and imaged using confocal microscopy. Two examples of infected cells displaying aberrant cytokinesis are shown (A to D and F to I). Viral proteins were labeled with the appropriate antibody and FITC and are shown in green (A and F), corresponding nuclei and nucleoli are stained with PI (red) (B and G), and the two images were superimposed (C and H). In addition, the corresponding bright-field images for the cells are depicted underneath (D and I). For orientation, in panels F and G, the nucleoli are denoted No and the cleavage furrow CF. Z-phase reconstruction was used to generate a section through the cell shown in panel C (E). For reference, the boundary of the nuclei is denoted B1 and B2, with the cleavage furrow as CF. The horizontal white line bisectioning the cell shown in panel C denotes the focal plane of the section. Magnification of all images is $\times 340$. (J) PI staining of a cell undergoing normal nuclear division. (K) Corresponding bright-field image. (L and M) IBV-infected cells displaying aberrant cytokinesis, with IBV proteins labeled in green and p53 in red. CF, cleavage furrow.

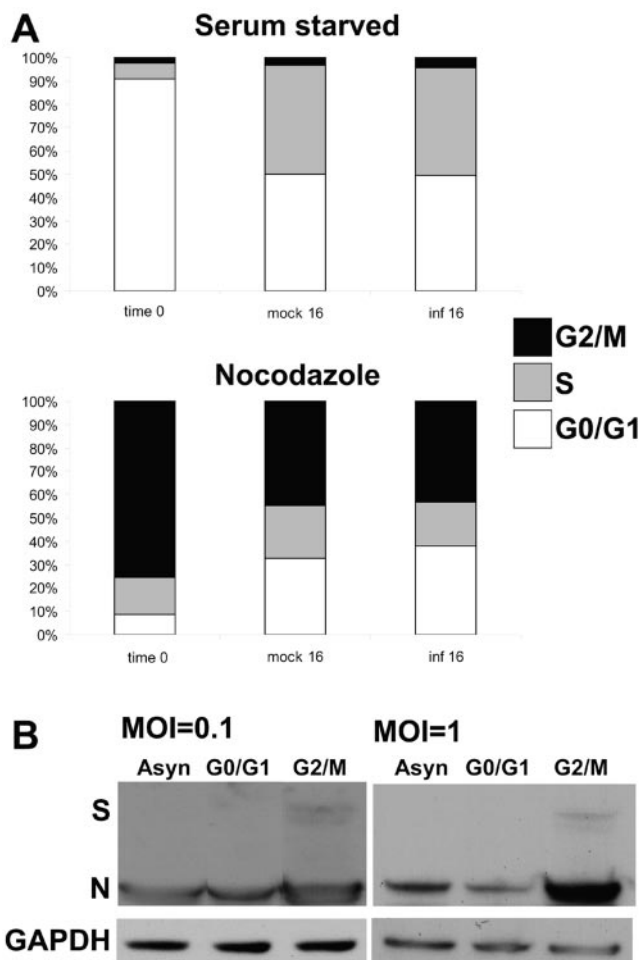


FIG. 6. (A) Cell cycle profiles of cells arrested in either the G₁ phase using serum starvation or the M phase using nocodazole. Following synchronization (time zero) cells were released from block and simultaneously mock infected and infected, and cell cycle profiles were analyzed 16 h later (mock 16 and inf 16, respectively). The y axis is the percentage of cells in the indicated phase of the cell cycle. The histograms show the means of three samples; similar results were obtained from three independent experiments. (B) Western blot analysis of viral proteins 16 h postinfection and release in asynchronously replicating cells (Asyn) and cells in G₀/G₁ and G₂/M blocked using serum starvation and nocodazole, respectively. Using the polyclonal anti-IBV antibody the N protein can be readily identified as well as the S protein.

3). Therefore, we investigated whether this stage of the cell cycle was advantageous for the virus by comparing virus protein accumulation as a marker for virus infection and virus titers as a marker for progeny virus production between subconfluent cells synchronized in the G₂/M phase and, as controls, cells synchronized in G₀/G₁ phase and asynchronously dividing cells. Following treatments approximately 90% cells were arrested in the G₀/G₁ phase by total serum deprivation (Fig. 6A) and, using nocodazole, approximately 75% of cells were arrested in the G₂/M phase (Fig. 6A). In asynchronous subconfluent Vero cells approximately 57% of cells were in G₀/G₁, 36% in S phase, and 7% in G₂/M phase. Cells were simultaneously released from their induced cell cycle block and either mock infected or infected with IBV at an MOI of 0.1 or

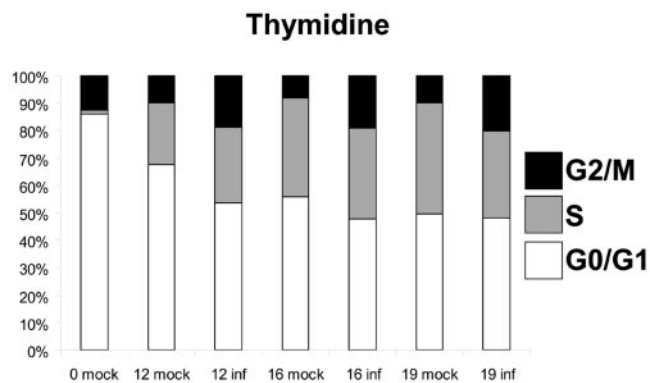


FIG. 7. Cell cycle profiles of cells arrested at the G₁/S phase border using double-thymidine treatment (*n* = 3). Following synchronization (time zero) cells were released from block and simultaneously mock infected and infected, and cell cycle profiles were analyzed at 12, 16, and 19 h p.i. (indicated below the appropriate bar). There was a significant increase in the number of IBV-infected cells in the G₂/M phase of the cell cycle compared to mock-infected cells at 12 h p.i. (*P* < 0.05, *n* = 3) and both 16 and 19 h p.i. (*P* < 0.01, *n* = 3). The y axis is the percentage of cells in the indicated phase of the cell cycle. Similar results were obtained from three independent experiments.

1, and the amount of viral protein accumulation was determined by Western blotting at 16 h postinfection. The cells were removed from their respective blocks so that the cells could reenter cell cycle progression. Protein lysates were prepared and equal amounts of protein resolved by SDS-polyacrylamide gel electrophoresis; this was confirmed by probing for GAPDH (Fig. 6B). Western blot analysis indicated that at 16 h postinfection the levels of virus protein accumulation were higher in G₂/M-synchronized cells than in G₀/G₁-synchronized and asynchronous replicating cells at both MOIs tested (Fig. 6B). For example, the levels of N protein accumulation were 1.5-fold and 4-fold higher in G₂/M-phase-synchronized cells infected at MOIs of 0.1 and 1, respectively, compared to N protein accumulation in the asynchronously replicating cells. Likewise the spike glycoprotein (S protein) was visible only in the G₂/M-phase-synchronized population at 16 h postinfection. Analysis of progeny virus production, at the latter MOI, at 16 h postinfection indicated there was greater progeny virus production in the G₂/M-phase-synchronized population ($[1.42 \pm 0.03] \times 10^5$ PFU/ml) compared to progeny virus in the asynchronous ($[6.79 \pm 0.10] \times 10^4$ PFU/ml) or G₀/G₁-phase-synchronized cells ($[4.17 \pm 0.42] \times 10^4$ PFU/ml).

Based upon infection of asynchronously replicating cells we hypothesized that IBV arrested cells in the G₂/M phase of the cell cycle. However, analysis of the cell cycle profiles from IBV-infected nocodazole-synchronized cells at 16 h postinfection and release revealed no G₂/M phase delay compared to mock-infected cells. To investigate this further, we synchronized cells at the G₁/S phase border using a double-thymidine block, which resulted in approximately 85% of cells being arrested at the G₁/S phase border. Infection of these cells and simultaneous release from block indicated that as the infected cells progressed through the cell cycle there was a significant delay of cells leaving the G₂/M phase compared to mock-infected cells (*P* < 0.05). Three independent experiments were performed in triplicate (Fig. 7).

DISCUSSION

In this study we demonstrated that IBV-infected cells accumulate in the G₂/M phase of the cell cycle, and the effect was not cell type specific and could be reproduced in synchronously replicating cells. This accumulation was dependent upon infection with replication-competent IBV, as UV-inactivated IBV was unable to induce a G₂/M phase arrest. We observed significant decreases in the levels of the D type cyclins between virus-infected and mock-infected cells. While there have been reports that coronavirus infection can result in a general decrease in cellular protein synthesis (18, 35), there have been no reports for this with IBV, and also inhibition of translation would not account for the above observations as there was no decrease in the levels of the cellular proteins GAPDH and PCNA, the latter of which is also regulated by the cell cycle (34). The reduced level of D type cyclins in infected cells may reflect the increased number of cells in the G₂/M phase of the cell cycle and the lack of progression to the G₁ phase, where cyclin D1 is expressed. In general, down-regulation of cyclin D1 in cells can result in reduced proliferation (14), and possible mechanisms for the reduction in cyclin D include degradation by the ornithine decarboxylase (ODC) regulatory protein ODC-antizyme (36). Reduced cell proliferation is observed in cells expressing N protein and coronavirus-infected cells (6, 58, 60). Our data indicate that, while the overall levels of p53 remained unchanged between virus-infected and mock-infected cells, the subcellular localization of p53 was altered, with p53 being present predominantly with punctate staining in the cytoplasm in infected cells compared to mock-infected cells. As a consequence of the redistribution of p53 IBV may delay the onset of apoptosis, which has been reported for IBV-infected cells (29). Certainly the redistribution of p53 to the cytoplasm in infected cells to delay or prevent p53-mediated apoptosis has been reported for a number of diverse viruses and viral proteins, including hepatitis C virus (HCV) NS5a protein (24) and adenovirus type 12 E1B protein (62).

In virus-infected Vero cells we observed apparent aberrant cytokinesis and reduced BrdU labeling, indicating potentially perturbed DNA synthesis. If DNA was damaged in virus-infected cells, rather than there being a reduced level of synthesis, then we may have predicted an increase in the levels of p53 and p21; however, we observed no increase in the levels of these proteins between virus-infected and mock-infected cells. We hypothesize that the reduction of BrdU uptake could be due to down-regulation of cellular DNA synthesis induced by infection, which could, subsequently, contribute to aberrant cytokinesis. Reduced DNA synthesis has been reported in cells infected with mouse hepatitis virus (MHV) (4). While binucleate cells can occur in continuously cultured cells, the frequency of this is approximately 3% (60), whereas in virus-infected cells it is on average 15%. These structures are not to be misinterpreted as small syncytia, which are visible as multinucleate cells; the structures we identify as evidence of aberrant cytokinesis are binucleate with the nuclei still fused together, albeit separated by a cleave furrow. The observation of aberrant cytokinesis and reduced DNA synthesis in virus-infected cells is very similar to results described in experiments investigating the function of eukaryotic origin recognition complex proteins 2 and 6, which are required for the initiation of DNA replica-

tion. RNA silencing studies showed a reduction of DNA synthesis, reduced BrdU staining of S phase cells, and various cytokinesis aberrations, as well as an accumulation of G₂/M phase cells (45–47).

Cell cycle perturbations have been reported for other coronaviruses. Chau et al. (3) conducted a morphological analysis of hepatocytes derived from liver specimens obtained from individuals infected with severe acute respiratory syndrome coronavirus and observed an increase in the number of hepatocytes undergoing mitosis. Chen and Makino (4) have shown that the murine coronavirus MHV can induce a G₀/G₁ phase arrest in virus-infected cells and that host cell DNA synthesis was down-regulated, although a different strain of MHV grew better in cells in the S phase (56). Our results are in similar agreement with Chen and Makino (4), except we observed an accumulation of cells in the G₂/M phase rather than the G₀/G₁ phase. In a subsequent analysis Chen et al. (5) reported that p21 levels appeared to be up-regulated in cells overexpressing the MHV replicase protein p28, although there appeared to be no significant difference in p21 levels in actual MHV-infected cells (4). The differences between our study and that of Chen and Makino (4) might be attributable to an inherent difference in the two coronaviruses or cell types or might partly reflect the difference in cell cycle analysis. Chen and Makino (4) determined cell cycle profiles using PI staining and the algorithm Modfit to assign the different cell cycle phases. This algorithm provides an estimate of the number of cells in the S phase of the cell cycle, whereas we measured this population directly using metabolic incorporation of BrdU.

The possible reason why coronaviruses in particular and positive-strand RNA viruses in general affect the cell cycle is not clearly understood. In the case of IBV this effect might consist of both altering host cell function and creating favorable conditions for virus replication. Several hypotheses have been advanced as to how arresting the cell cycle at a specific stage may promote RNA virus infection; these include increasing the efficiency of replication, translation, and virus assembly. Scholle et al. (53) demonstrated that, while expression of the HCV polyprotein did not cause arrest in any particular stage of the cell cycle, HCV RNA synthesis was enhanced in S phase compared to serum-starved, contact-inhibited, or poorly proliferating cells. In the case of those positive-strand RNA viruses whose protein synthesis is under the control of a defined internal ribosomal entry site (IRES), there might be an advantage for the virus to arrest cells in the G₂/M phase of the cell cycle, in which IRES-dependent translation of some (but not all) cellular (7, 49, 50, 59) and certain viral mRNAs (19) has been reported to be optimal compared to other stages of the cell cycle. While the translation of one coronavirus, including IBV, protein is thought to be dependent on IRES-like activity (21, 25, 30, 31, 39), this is not true for the remainder of the viral proteins, which are thought to be translated via cap-dependent mechanisms (23). Lin and Lamb (28) proposed that enveloped RNA viruses could arrest the cell cycle before mitosis to prevent disruption of the Golgi apparatus and endoplasmic reticulum (ER), favoring viruses whose assembly occurs in these structures. Certainly coronaviruses such as IBV utilize the Golgi apparatus and ER for protein processing and assembly (1, 27, 32, 33).

To specifically investigate whether a particular stage of the

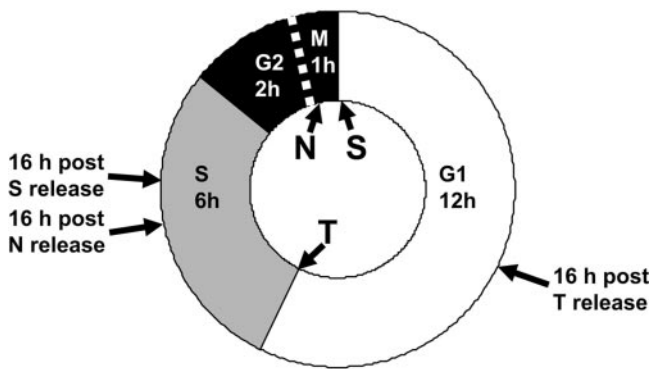


FIG. 8. Diagrammatic representation of the length of each cell cycle stage in asynchronously cycling Vero cells. G_1 phase (white) takes approximately 12 h, S phase (gray) takes approximately 6 h, and G_2 and M phases (black) take approximately 2 and 1 h to complete, respectively. The points in the cell cycle where serum starvation (S), the double-thymidine block (T), and nocodazole (N) block the cell cycle are indicated. On the outside is indicated where in the cell cycle synchronously replicating cells reach when released from their appropriate block.

cell cycle favored virus replication, we arrested cells in various stages of the cell cycle and compared efficiencies of virus infection. We showed that IBV efficiency as determined by increased protein accumulation and progeny virus production is greater in cells enriched in the G_2/M phase of the cell cycle at 16 h postinfection when compared to either cells enriched in the G_0/G_1 phase or asynchronously replicating cells. Both of these markers are larger in asynchronously replicating cells compared to cells enriched in the G_0/G_1 phase and may be a reflection of the greater number of cells in the G_2/M phase found in asynchronously replicating cells compared to cells arrested by serum starvation. These data indicated protein synthesis was greater in G_2/M phase, which most likely had a knock-on effect for virus assembly and hence increased virus output. Curiously, cap-dependent translation has been reported to be down-regulated in the G_2/M phase of the cell cycle, suggesting either that IBV may use a cellular factor(s) which is optimally expressed in G_2/M to enhance virus translation or that the coronavirus N protein or leader sequence might carry out this role (54, 55). HIV infection is also favored in the G_2/M phase, and Groschel and Bushman (12) observed a three- to fivefold increase in HIV transduction compared to other stages of the cell cycle. In contrast, coxsackievirus (B3) production was 10- to 100-fold lower in cells arrested in G_2/M when compared to cells arrested either in G_1 or at the G_2/S phase boundary (10). This is in contrast to the hypothesis that IRES-dependent translation is favored in the G_2/M phase.

While we observed an increase in virus growth (in terms of virus protein accumulation and progeny virus production) in cells enriched in the G_2 phase of the cell cycle using treatment with nocodazole, we did not observe a corresponding delay of infected cells leaving the G_2/M phase. This observation was unexpected because based on the data generated from asynchronously replicating cells we would have predicted this. However, nocodazole arrests cells at the G_2/M boundary/early M phase, and therefore if the mechanism of IBV-induced block/delay is initiated before this point in the cell cycle then

we would not observe any difference in the G_2/M phase populations between mock-infected and infected cells (Fig. 8). To further investigate this, we synchronized cells at the G_1/S phase border using a double-thymidine block. Infection of cells blocked and released at this point indicated an accumulation of cells in the G_2/M phase compared to mock-infected cells. Overall our data show that IBV induces a G_2/M phase perturbation in both asynchronously and synchronously replicating cells, and therefore we favor the hypothesis that IBV induces a G_2/M phase cell cycle arrest in order to promote conditions for progeny virus production.

ACKNOWLEDGMENTS

This work was funded by the BBSRC (grant number BBS/B/03416) to J.A.H. and G.B. The confocal microscope facility in the Astbury Centre for Structural Molecular Biology was funded by the Wellcome Trust and SRIF. The flow cytometer at the University of Leeds was provided by a grant from Yorkshire Cancer Research.

We thank Gareth Howell for his help in using the confocal microscope facility. We acknowledge the help and expertise of Graham Botley of the University of Leeds and Carmen Coxon and Jane Harper of the University of Reading with the flow cytometry.

REFERENCES

- Alonso-Caplen, F. V., Y. Matsuoka, G. E. Wilcox, and R. W. Compans. 1984. Replication and morphogenesis of avian coronavirus in Vero cells and their inhibition by monensin. *Virus Res.* **1**:153-167.
- Casais, R., B. Dove, D. Cavanagh, and P. Britton. 2003. Recombinant avian infectious bronchitis virus expressing a heterologous spike gene demonstrates that the spike protein is a determinant of cell tropism. *J. Virol.* **77**:9084-9089.
- Chau, T. N., K. C. Lee, H. Yao, T. Y. Tsang, T. C. Chow, Y. C. Yeung, K. W. Choi, Y. K. Tso, T. Lau, S. T. Lai, and C. L. Lai. 2004. SARS-associated viral hepatitis caused by a novel coronavirus: report of three cases. *Hepatology* **39**:302-310.
- Chen, C. J., and S. Makino. 2004. Murine coronavirus replication induces cell cycle arrest in G_0/G_1 phase. *J. Virol.* **78**:5658-5669.
- Chen, C. J., K. Sugiyama, H. Kubo, C. Huang, and S. Makino. 2004. Murine coronavirus nonstructural protein p28 arrests cell cycle in G_0/G_1 phase. *J. Virol.* **78**:10410-10419.
- Chen, H., T. Wurm, P. Britton, G. Brooks, and J. A. Hiscox. 2002. Interaction of the coronavirus nucleoprotein with nucleolar antigens and the host cell. *J. Virol.* **76**:5233-5250.
- Cornelis, S., Y. Bruynooghe, G. Denecker, S. Van Huffel, S. Tinton, and R. Beyaert. 2000. Identification and characterization of a novel cell cycle-regulated internal ribosome entry site. *Mol. Cell* **5**:597-605.
- Darzynkiewicz, Z., E. Bedner, and P. Smolewski. 2001. Flow cytometry in analysis of cell cycle and apoptosis. *Semin. Hematol.* **38**:179-193.
- Dolbeare, F., H. Gratzner, M. G. Pallavicini, and J. W. Gray. 1983. Flow cytometric measurement of total DNA content and incorporated bromodeoxyuridine. *Proc. Natl. Acad. Sci. USA* **80**:5573-5577.
- Feuer, R., I. Mena, R. Pagarigan, M. K. Slifka, and J. L. Whitton. 2002. Cell cycle status affects coxsackievirus replication, persistence, and reactivation in vitro. *J. Virol.* **76**:4430-4440.
- Goh, W. C., M. E. Rogel, C. M. Kinsey, S. F. Michael, P. N. Fultz, M. A. Nowak, B. H. Hahn, and M. Emerman. 1998. HIV-1 Vpr increases viral expression by manipulation of the cell cycle: a mechanism for selection of Vpr *in vivo*. *Nat. Med.* **4**:65-71.
- Groschel, B., and F. Bushman. 2005. Cell cycle arrest in G_2/M promotes early steps of infection by human immunodeficiency virus. *J. Virol.* **79**:5695-5704.
- Guertin, D. A., S. Trautmann, and D. McCollum. 2002. Cytokinesis in eukaryotes. *Microbiol. Mol. Biol. Rev.* **66**:155-178.
- Han, E. K., S. C. Ng, N. Arber, M. Begemann, and I. B. Weinstein. 1999. Roles of cyclin D1 and related genes in growth inhibition, senescence and apoptosis. *Apoptosis* **4**:213-219.
- Harper, J. V. 2005. Synchronization of cell populations in G_1/S and G_2/M phases of the cell cycle. *Methods Mol. Biol.* **296**:157-166.
- He, J., S. Choe, R. Walker, P. Di Marzio, D. O. Morgan, and N. R. Landau. 1995. Human immunodeficiency virus type 1 protein R (Vpr) blocks cells in the G_2 phase of the cell cycle by inhibiting p34^{cdc2} activity. *J. Virol.* **69**:6705-6711.
- He, R., A. Leeson, A. Andonov, Y. Li, N. Bastien, J. Cao, C. Osioy, F. Dobie, T. Cutts, M. Ballantine, and X. Li. 2003. Activation of AP-1 signal transduction pathway by SARS coronavirus nucleocapsid protein. *Biochem. Biophys. Res. Commun.* **311**:870-876.

18. Hilton, A., L. Mizzen, G. MacIntyre, S. Cheley, and R. Anderson. 1986. Translational control in murine hepatitis virus infection. *J. Gen. Virol.* **67**: 923–932.
19. Honda, M., S. Kaneko, E. Matsushita, K. Kobayashi, G. A. Abell, and S. M. Lemon. 2000. Cell cycle regulation of hepatitis C virus internal ribosomal entry site-directed translation. *Gastroenterology* **118**:152–162.
20. Hrimech, M., X.-J. Yao, P. E. Branton, and E. A. Cohen. 2000. Human immunodeficiency virus type 1 Vpr-mediated G₂ cell cycle arrest: Vpr interferes with cell cycle signaling cascades by interacting with the B subunit of serine/threonine protein phosphatase 2A. *EMBO J.* **19**:3956–3967.
21. Jendrach, M., V. Thiel, and S. Siddell. 1999. Characterization of an internal ribosome entry site within mRNA 5' of murine hepatitis virus. *Arch. Virol.* **144**:921–933.
22. Kashanchi, F., E. T. Agbottah, C. A. Pise-Masison, R. Mahieux, J. Duvall, A. Kumar, and J. N. Brady. 2000. Cell cycle-regulated transcription by the human immunodeficiency virus type 1 Tat transactivator. *J. Virol.* **74**:652–660.
23. Lai, M. M., and S. A. Stohlman. 1981. Comparative analysis of RNA genomes of mouse hepatitis viruses. *J. Virol.* **38**:661–670.
24. Lan, K. H., M. L. Sheu, S. J. Hwang, S. H. Yen, S. Y. Chen, J. C. Wu, Y. J. Wang, N. Kato, M. Omata, F. Y. Chang, and S. D. Lee. 2002. HCV NS5A interacts with p53 and inhibits p53-mediated apoptosis. *Oncogene* **21**:4801–4811.
25. Le, S. Y., N. Sonenberg, and J. V. Maizel, Jr. 1994. Distinct structural elements and internal entry of ribosomes in mRNA3 encoded by infectious bronchitis virus. *Virology* **198**:405–411.
26. Levine, A. J. 1997. p53, the cellular gatekeeper for growth and division. *Cell* **88**:323–331.
27. Lim, K. P., and D. X. Liu. 2001. The missing link in coronavirus assembly. Retention of the avian coronavirus infectious bronchitis virus envelope protein in the pre-Golgi compartments and physical interaction between the envelope and membrane proteins. *J. Biol. Chem.* **276**:17515–17523.
28. Lin, G. Y., and R. A. Lamb. 2000. The paramyxovirus simian virus 5 V protein slows progression of the cell cycle. *J. Virol.* **74**:9152–9166.
29. Liu, C., H. Y. Xu, and D. X. Liu. 2001. Induction of caspase-dependent apoptosis in cultured cells by the avian coronavirus infectious bronchitis virus. *J. Virol.* **75**:6402–6409.
30. Liu, D. X., D. Cavanagh, P. Green, and S. C. Inglis. 1991. A polycistronic messenger-RNA specified by the coronavirus infectious bronchitis virus. *Virology* **184**:531–544.
31. Liu, D. X., and S. C. Inglis. 1992. Internal entry of ribosomes on a tricistronic mRNA encoded by infectious bronchitis virus. *J. Virol.* **66**:6143–6154.
32. Lontok, E., E. Corse, and C. E. Machamer. 2004. Intracellular targeting signals contribute to localization of coronavirus spike proteins near the virus assembly site. *J. Virol.* **78**:5913–5922.
33. Machamer, C. E., S. A. Mentone, J. K. Rose, and M. G. Farquhar. 1990. The E1 glycoprotein of an avian coronavirus is targeted to the *cis*-Golgi complex. *Proc. Natl. Acad. Sci. USA* **87**:6944–6948.
34. Madsen, P., and J. E. Celis. 1985. S-phase patterns of cyclin (PCNA) antigen staining resemble topographical patterns of DNA synthesis. A role for cyclin in DNA replication? *FEBS Lett.* **193**:5–11.
35. Mizzen, L., G. Macintyre, F. Wong, and R. Anderson. 1987. Translational regulation in mouse hepatitis virus infection is not mediated by altered intracellular ion concentrations. *J. Gen. Virol.* **68**:2143–2151.
36. Newman, R. M., A. Mobscher, U. Mangold, C. Koike, S. Diah, M. Schmidt, D. Finley, and B. R. Zetter. 2004. Antizyme targets cyclin D1 for degradation. A novel mechanism for cell growth repression. *J. Biol. Chem.* **279**: 41504–41511.
37. Nikolaev, A. Y., M. Li, N. Puskas, J. Qin, and W. Gu. 2003. Parc: a cytoplasmic anchor for p53. *Cell* **112**:29–40.
38. Nunez, R. 2001. DNA measurement and cell cycle analysis by flow cytometry. *Curr. Issues Mol. Biol.* **3**:67–70.
39. O'Connor, J. B., and D. A. Brian. 2000. Downstream ribosomal entry for translation of coronavirus TGEV gene 3b. *Virology* **269**:172–182.
40. Ormerod, M. G. 1994. Analysis of DNA—general considerations, p. 83–97. *In* M. Pagano (ed.), *Flow cytometry: a practical approach*, 3rd ed. Oxford University Press, New York, N.Y.
41. Ormerod, M. G., A. W. Payne, and J. V. Watson. 1987. Improved program for the analysis of DNA histograms. *Cytometry* **8**:637–641.
42. Pendleton, A. R., and C. E. Machamer. 2005. Infectious bronchitis virus 3a protein localizes to a novel domain of the smooth endoplasmic reticulum. *J. Virol.* **79**:6142–6151.
43. Pines, J. 1999. Four-dimensional control of the cell cycle. *Nat. Cell Biol.* **1**:73–79.
44. Planelles, V., J. B. M. Jowett, Q. X. Li, Y. Xie, B. Hahn, and I. S. Y. Chen. 1996. Vpr-induced cell cycle arrest is conserved among primate lentiviruses. *J. Virol.* **70**:2516–2524.
45. Prasanth, S. G., J. Mendez, K. V. Prasanth, and B. Stillman. 2004. Dynamics of pre-replication complex proteins during the cell division cycle. *Philos. Trans. R. Soc. Lond. B Biol. Sci.* **359**:7–16.
46. Prasanth, S. G., K. V. Prasanth, K. Siddiqui, D. L. Spector, and B. Stillman. 2004. Human Orc2 localizes to centrosomes, centromeres and heterochromatin during chromosome inheritance. *EMBO J.* **23**:2651–2663.
47. Prasanth, S. G., K. V. Prasanth, and B. Stillman. 2002. Orc6 involved in DNA replication, chromosome segregation, and cytokinesis. *Science* **297**: 1026–1031.
48. Prelich, G., C. K. Tan, M. Kostura, M. B. Mathews, A. G. So, K. M. Downey, and B. Stillman. 1987. Functional identity of proliferating cell nuclear antigen and a DNA polymerase-delta auxiliary protein. *Nature* **326**:517–520.
49. Pyronnet, S., L. Pradayrol, and N. Sonenberg. 2000. A cell cycle-dependent internal ribosome entry site. *Mol. Cell* **5**:607–616.
50. Qin, X., and P. Sarnow. 2004. Preferential translation of internal ribosome entry site-containing mRNAs during the mitotic cycle in mammalian cells. *J. Biol. Chem.* **279**:13721–13728.
51. Re, F., D. Braaten, E. K. Franke, and J. Luban. 1995. Human immunodeficiency virus type 1 Vpr arrests the cell cycle in G₂ by inhibiting the activation of p34^{cdc2}-cyclin B. *J. Virol.* **69**:6859–6864.
52. Rubbi, C. P., and J. Milner. 2003. Disruption of the nucleolus mediates stabilization of p53 in response to DNA damage and other stresses. *EMBO J.* **22**:6068–6077.
53. Scholle, F., K. Li, F. Bodola, M. Ikeda, B. A. Luxon, and S. M. Lemon. 2004. Virus-host cell interactions during hepatitis C virus RNA replication: impact of polyprotein expression on the cellular transcriptome and cell cycle association with viral RNA synthesis. *J. Virol.* **78**:1513–1524.
54. Tahara, S. M., T. A. Dietlin, C. C. Bergmann, G. W. Nelson, S. Kyuwa, R. P. Anthony, and S. A. Stohlman. 1994. Coronavirus translational regulation: leader affects mRNA efficiency. *Virology* **202**:621–630.
55. Tahara, S. M., T. A. Dietlin, G. W. Nelson, S. A. Stohlman, and D. J. Manno. 1998. Mouse hepatitis virus nucleocapsid protein as a translational effector of viral mRNAs. *Adv. Exp. Med. Biol.* **440**:313–318.
56. Talbot, P. J., and C. Daniel. 1987. Influence of the cell cycle on the infectious titer of murine hepatitis virus, strain A59. *Adv. Exp. Med. Biol.* **218**:267–268.
57. Taylor, W. R., and G. R. Stark. 2001. Regulation of the G₂/M transition by p53. *Oncogene* **20**:1803–1815.
58. Timani, K. A., Q. Liao, L. Ye, Y. Zeng, J. Liu, Y. Zheng, X. Yang, K. Lingbao, J. Gao, and Y. Zhu. 2005. Nuclear/nucleolar localization properties of C-terminal nucleocapsid protein of SARS coronavirus. *Virus Res.* **114**:23–34.
59. Tinton, S. A., B. Schepens, Y. Bruynooghe, R. Beyaert, and S. Cornelis. 2005. Regulation of the cell-cycle-dependent internal ribosome entry site of the PITSLRE protein kinase: roles of Unr (upstream of N-ras) protein and phosphorylated translation initiation factor eIF-2 α . *Biochem. J.* **385**:155–163.
60. Wurm, T., H. Chen, P. Britton, G. Brooks, and J. A. Hiscox. 2001. Localization to the nucleolus is a common feature of coronavirus nucleoproteins, and the protein may disrupt host cell division. *J. Virol.* **75**:9345–9356.
61. Youn, S., J. L. Leibowitz, and E. W. Collisson. 2005. In vitro assembled, recombinant infectious bronchitis viruses demonstrate that the 5a open reading frame is not essential for replication. *Virology* **332**:206–215.
62. Zhao, L. Y., and D. Liao. 2003. Sequestration of p53 in the cytoplasm by adenovirus type 12 E1B 55-kilodalton oncoprotein is required for inhibition of p53-mediated apoptosis. *J. Virol.* **77**:13171–13181.